NASA TECHNICAL NOTE

NASA TN D-5343

c. 1

NASA TN D-5343

SHOCK SHAPES AND PRESSURE DISTRIBUTIONS FOR LARGE-ANGLE POINTED CONES IN HELIUM AT MACH NUMBERS OF 8 AND 20

by David A. Stewart and Mamoru Inouye

Ames Research Center
Moffett Field, Calif.

NATIONAL AERONAUTICS AND SPACE ADMINISTRATION • WASHINGTON, D. C. • JULY 1969

SHOCK SHAPES AND PRESSURE DISTRIBUTIONS FOR LARGE-ANGLE POINTED CONES IN HELIUM AT MACH NUMBERS OF 8 AND 20

By David A. Stewart and Mamoru Inouye

Ames Research Center
Moffett Field, Calif.

NATIONAL AERONAUTICS AND SPACE ADMINISTRATION

For sale by the Clearinghouse for Federal Scientific and Technical Information
Springfield, Virginia 22151 – CFSTI price $3.00

SHOCK SHAPES AND PRESSURE DISTRIBUTIONS FOR LARGE-ANGLE POINTED CONES IN HELIUM AT MACH NUMBERS OF 8 AND 20

By David A. Stewart and Mamoru Inouye

Ames Research Center

SUMMARY

Bow-wave shapes and surface pressures were measured in helium at Mach numbers 8 and 20 on pointed cones with semivertex angles from 52° to 90°. For large cone angles ($\geq$ 65°) the bow wave was nearly spherical, the bow-wave shape and surface pressure distribution were predicted adequately by both the method of integral relations and the method of Kaattari, and the bow-wave shape was not influenced by cone angle or small amount of bluntness. For cone angles approaching shock attachment (attachment < δ < 65°) where the bow wave was no longer spherical, the method of integral relations adequately predicted the shock shape and surface pressure distribution. The Kaattari method was not applicable for these conditions.

INTRODUCTION

The conical body at zero angle of attack has been a basic shape in supersonic aerodynamic research for which much theoretical and experimental data has been accumulated over the years.

For pointed cones with vertex angles small enough for an attached shock wave, the well-known conical flow solutions are applicable (refs. 1-4) and well substantiated by experiments. For large vertex angles where the bow wave is detached, no exact solutions exist, and very little experimental work is reported in the literature.

For blunt cones, the bow wave is always detached. However, for small vertex angles, it is possible to solve numerically for the flow field in the subsonic-transonic region by an inverse method and the flow field in the supersonic region by the method of characteristics (ref. 5). The results agree generally with experimental results. For large vertex angles with subsonic flow on the conical surface no exact solutions exist, but some experimental results have been reported (refs. 6, 7). Approximate methods for predicting the flow fields include the method of integral relations (refs. 8, 9) and the Kaattari method (refs. 10, 11).

The present investigation was initiated to study the hypersonic flow of helium around pointed cones with large vertex angles and detached bow waves.

The purpose of this report is to present the experimental data (shadowgraphs of the bow waves and surface pressure distributions) and to evaluate the extension of the aforementioned approximate methods to pointed cones.

SYMBOLS

D	distance from sonic point on body to apex of shock wave, measured parallel to the body axis (fig. 1)
M	Mach number
p	pressure
R	radius
Re	Reynolds number based on free-stream conditions
s	distance along surface measured from the apex
T	absolute temperature
x,y	cylindrical coordinates
Δ	shock-wave standoff distance, measured parallel to the body axis
δ	cone semivertex angle

Subscripts

*	sonic point
o	centerline
t	total free-stream conditions
b	base of body
n	nose of body
∞	free stream
t_2	stagnation conditions behind normal shock

TEST APPARATUS AND CONDITIONS

Facility

The tests were conducted in the Ames hypersonic helium tunnel, which is a closed-circuit, blowdown tunnel with contoured nozzles and with run times of 1/2 to 2 minutes. The facility is described in reference 12. The shadowgraph system is of the single-path spark-gap type with a 0.004-inch-diameter orifice at the source.

The tests were performed at free-stream Mach numbers of 8 and 20 under the following conditions:

M_∞	p_t, psia	T_t, °R	Re/in.
8	150	530	2.4×10^5
20	2000	530	7.0×10^5

Models

The shapes tested were pointed cones with semivertex angles between 52° and 90°. A typical body is shown in figure 1. The model consisted of a conical test surface with a short cylindrical afterbody 2.25 inches in diameter.

Surface pressures were measured with bonded strain-gage transducers connected to 0.040-inch-diameter orifices at three locations (fig. 1). The exact locations varied with the cone angle, as indicated in the pressure distributions shown later. The stagnation-point pressure was measured with a separate probe in the tunnel.

APPROXIMATE PREDICTION METHODS

The flow field around a blunt cone with subsonic flow over the surface may be predicted by the method of integral relations or the Kaattari method. Both methods are applied herein to a pointed cone.

The method of integral relations, based on Belotserkovskii's work (ref. 8), solves the equations of motion for inviscid flow with the assumption that the flow properties across the shock layer may be represented by polynomials. For the one-strip solutions presented in this report, the polynomials reduce to straight lines. A brief discussion of the method may be found in reference 9. Since the method requires a rounded nose with a stagnation point at the centerline, solutions for a pointed cone may be approximated if the cone is considered to be blunt and to have a very small nose radius. A nose-to-base-radius ratio, R_n/R_b, equal to 0.01 was used in the calculations in this report.

The Kaattari method (refs. 10 and 11) is a semiempirical approach that assumes a spherical bow wave with standoff distances at the centerline and at the sonic point obtained from empirical correlations. Surface pressure distributions are then determined by means of continuity relations. Solutions for a pointed cone, in this case, may be approximated if the cone is assumed to be a spherical segment with the same inclination angle at the sonic point as the pointed cone. This configuration represents the limiting case of a cone with maximum nose bluntness; for example, $R_n/R_b = 2$ for a 60° semivertex angle cone and $R_n/R_b = \infty$ for a flat-faced cylinder (90° semivertex cone).

RESULTS AND DISCUSSION

The experimentally determined bow-wave shapes and surface-pressure distributions are presented in figures 2 through 6. These data are compared with the predictions of the method of integral relations and the Kaattari method. Bow-wave parameters of particular interest are the standoff distances at the centerline and at the sonic point.

Shock-Wave Shape

Shadowgraphs of the bow wave are shown in figure 2 for $52° \leq \delta \leq 90°$ and for $M_\infty = 8$ and 20. Bow-wave detachment appears to occur at a cone half-angle between 52° and 55°. In reference 4, the detachment angle for pointed cones at $M = 20$ is given as 50.6°. The difference in detachment angle may be attributed to the fact that the tested cones are of finite length and thus the subsonic flow behind the bow wave is affected by the corner. The geometry of the bow wave for the pointed cones can be divided into two regimes from figure 2: (1) nonspherical bow-wave shapes near the attachment angle ($52° < \delta < 65°$), and (2) spherical bow-wave shapes at large cone angles ($\delta \geq 65°$). For the same cone angle, the bow-wave shapes for $M_\infty = 8$ and 20 are similar, with the bow wave being slightly closer to the body for the higher Mach number.

Bow-wave coordinates read from the shadowgraphs are compared in figure 3 with predictions of the integral and Kaattari methods. Results from the integral method for $M_\infty = 20$ (solutions for $M_\infty = 8$ are essentially identical) agree well with the experimental data for $55° < \delta < 80°$. For $\delta = 90°$, the predicted bow-wave shape is noticeably closer to the body than the measured shape. For $\delta = 52°$, no solution was obtained because of the proximity to shock attachment. Results of the Kaattari method agree well with the experimental data for $\delta \geq 65°$, where the bow wave is spherical. For $\delta \leq 58°$, agreement between the Kaattari method and experiment is poor because the effects of nose geometry are significant and the body shape can no longer be approximated by a spherical segment.

The shock standoff distance at the centerline is shown in figure 4 to increase almost linearly with cone angle. This variation has been previously observed experimentally by Johnson (ref. 6) and theoretically by South (ref. 13). The predictions from the method of integral relations and the

Kaattari method also show this behavior except for $\delta < 65°$, where the latter method is not applicable because of the difference in the nose shape.

The shock standoff distance opposite the sonic corner, Δ_*, and the distance from the sonic corner to the apex of the bow wave, D, are shown in figure 5 as functions of cone angle. These data show, in particular, that the normalized distance, Δ_*/R_b, is essentially independent of δ. This result is consistent with a mass balance at the sonic point where the free-stream mass entering through the area, πR_b^2, must equal the shock-layer mass leaving through the area, $2\pi R_b \Delta_*$. Since the flow conditions within the shock layer near the sonic point are also nearly sonic and thus independent of δ, it follows that Δ_*/R_b should also be independent of δ. These data also show that the normalized distance, D/R_b, is independent of δ when the bow wave is spherical ($\delta \geq 65°$), but that it decreases with δ near the shock detachment regime. Values of D/R_b obtained by Johnson (ref. 6) for blunted cones with $R_n/R_b = 0.3$ are also shown in figure 5 and agree well with the present results. It can be concluded from these data (fig. 5) that when the bow wave becomes spherical ($\delta \geq 65°$) the shape of the bow wave is not appreciably affected by either cone angle or small amounts of bluntness. The two prediction methods show reasonable agreement with the experimental data.

Surface Pressure Distributions

Surface pressures measured at three locations on the cone are shown in figure 6 for $52° \leq \delta \leq 80°$ and for $M_\infty = 8$ and 20. As the cone angle increases, the surface pressure level rises to the stagnation-point value. The method of integral relations shows good agreement with the data for all cases in which it could be applied (i.e., $\delta \geq 55°$), and the Kaattari method shows good agreement for $\delta \geq 65°$. The fluctuations in the pressure near the tip for the method of integral relations are due to the small nose bluntness. Modified Newtonian theory predicts the mean of the measured values for $\delta = 65°$ and 70°, but is low for smaller cone angles and high for larger cone angles.

CONCLUSIONS

Bow-wave shapes and surface pressure distributions were measured in helium at Mach numbers 8 and 20 on pointed cone models with semivertex angles from 52° to 90°. The data were compared with results from two approximate prediction methods. The investigation resulted in the following conclusions:

1. For large cone angles (semivertex angles 65° or greater) the bow wave was nearly spherical and only slightly affected by changes in cone angle and nose bluntness. For $\delta \geq 65°$, the bow-wave shapes and surface pressure distributions were predicted adequately by both the method of integral relations and the Kaattari method.

2. For cone angles approaching the condition of shock attachment (semivertex angles less than 65°), the bow wave was no longer spherical but changed appreciably with cone angle. For these cone angles, the bow-wave shape and surface pressure distribution were predicted adequately by the method of integral relations. The Kaattari method was not applicable for these cone angles.

Ames Research Center
National Aeronautics and Space Administration
Moffett Field, Calif., 94035, Apr. 22, 1969

REFERENCES

1. Taylor, G. I.; and MacColl, J. W.: The Air Pressure on a Cone Moving at High Speeds. Proc. Roy. Soc. (London), Ser. A139, 1933, pp. 278-311.

2. Staff of the Computing Section, Center of Analysis (Under Direction of Zdenek Kopal): Tables of Supersonic Flow Around Yawing Cones. Tech. Rept. 3, MIT, Cambridge, Mass., 1947.

3. Sims, J. L.: Tables for Supersonic Flow Around Right Circular Cones at Zero Angle of Attack. NASA SP-3004, 1964.

4. Mueller, James N.: Equations, Tables, and Figures for Use in the Analysis of Helium Flow at Supersonic and Hypersonic Speeds. NACA TN 4063, 1957.

5. Inouye, Mamoru; Rakich, John V.; and Lomax, Harvard: A Description of Numerical Methods and Computer Programs for Two-Dimensional and Axisymmetric Supersonic Flow Over Blunt-Nosed and Flared Bodies. NASA TN D-2970, 1965.

6. Johnson, Robert H.: The Cone-Sphere in Hypersonic Helium Above Mach 20. Aero. and Space Engineering, Feb. 1959. (Also available as IAS Rept. 59-2.)

7. Saida, Nobumi: Supersonic Flow Around Blunt Cones at Small Angles of Attack. Trans. Japan Soc. for Aeronautical and Space Sciences, vol. 8, no. 13, 1965, pp. 45-53.

8. Belotserkovskii, O. M. (J. F. Springfield, trans. and ed.): The Calculation of Flow Over Axisymmetric Bodies With a Detached Shock Wave. Computation Center, Acad. Sci., Moscow, USSR, 1961. RAD-TM-62-64, AVCO Corp., 1962.

9. Inouye, Mamoru; Marvin, Joseph G.; and Sinclair, A. Richard: Comparison of Experimental and Theoretical Shock Shapes and Pressure Distributions on Flat-Faced Cylinders at Mach 10.5. NASA TN D-4397, 1968.

10. Kaattari, George E.: Predicted Shock Envelopes About Two Types of Vehicles at Large Angles of Attack. NASA TN D-860, 1961.

11. Kaattari, George E.: Predicted Gas Properties in the Shock Layer Ahead of Capsule-Type Vehicles at Angles of Attack. NASA TN D-1423, 1962.

12. Tendeland, Thorval; and Pearson, Byrd D.: Effectiveness of the Flap Controls on a Mercury Type Capsule at a Mach Number of 15 in the Ames Hypersonic Helium Tunnel. NASA TM X-660, 1962.

13. South, Jerry C., Jr: Calculation of Axisymmetric Supersonic Flow Past Blunt Bodies With Sonic Corners, Including a Program Description and Listing. NASA TN D-4563, 1968.

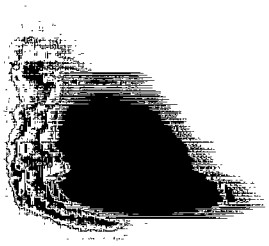

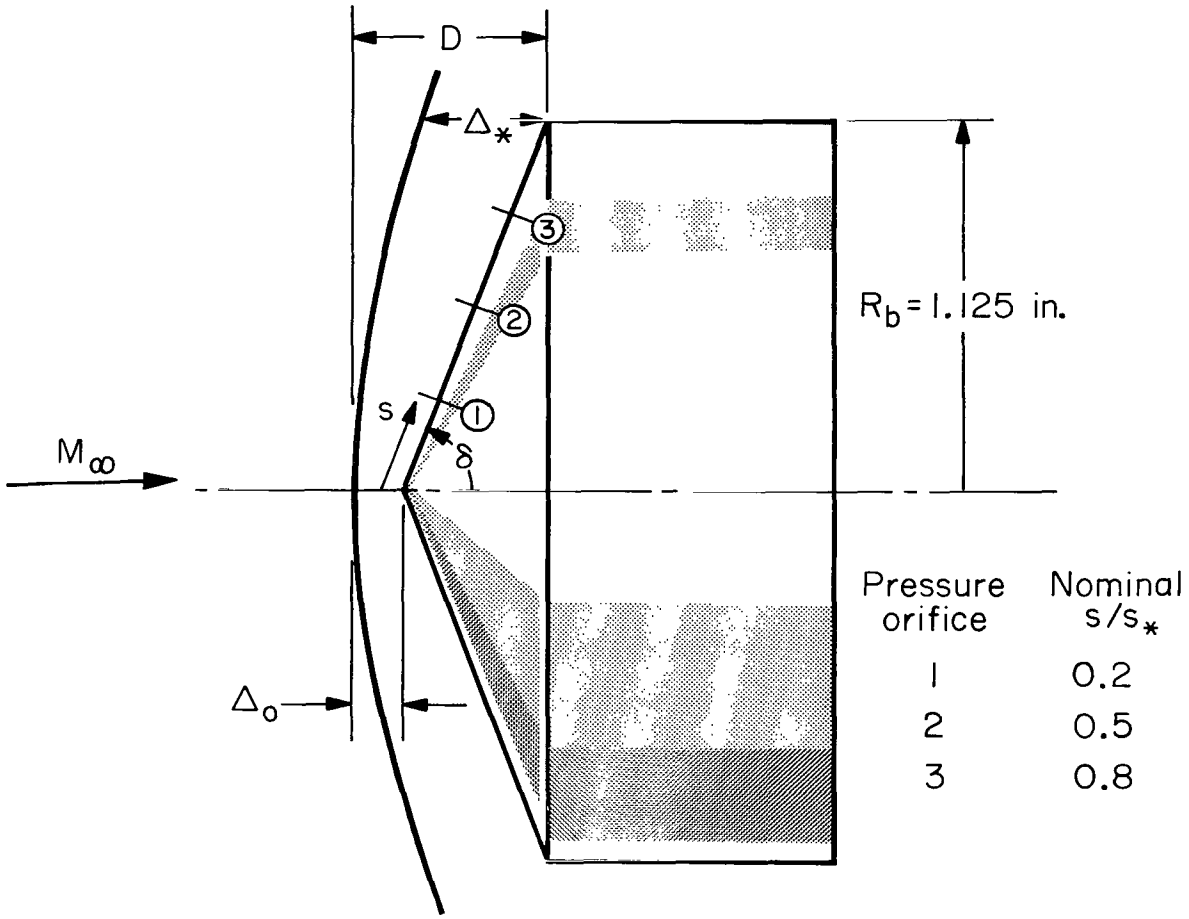

Figure 1.- Typical model configuration.

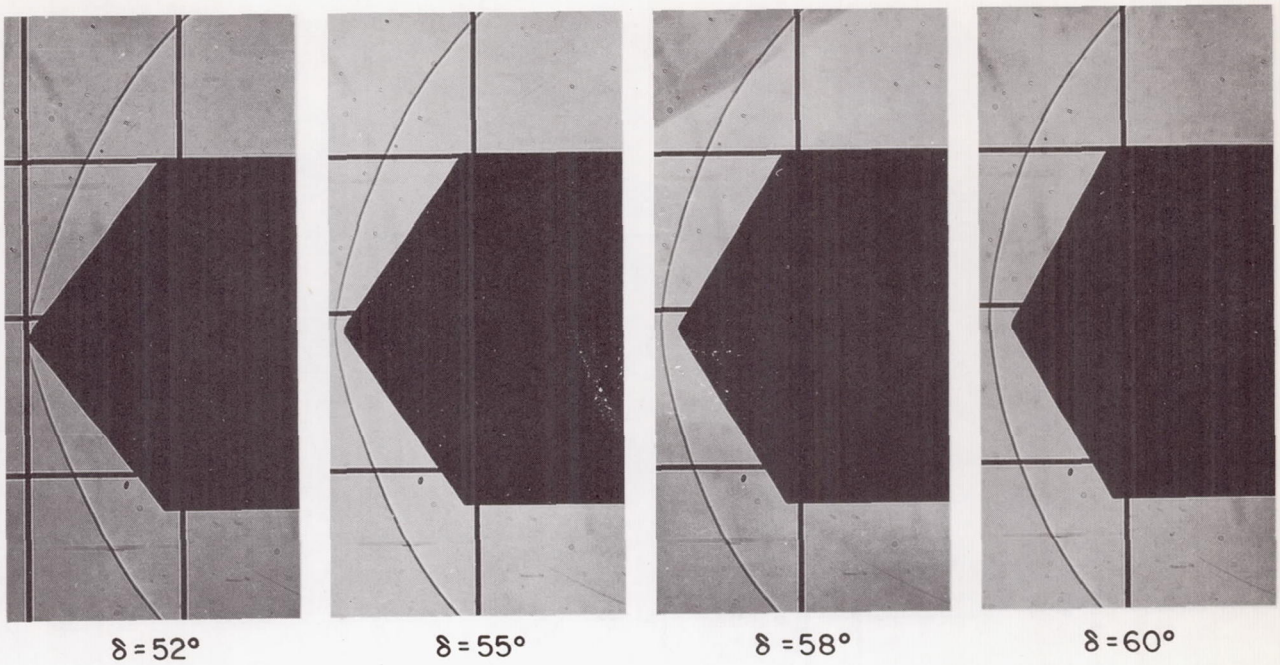

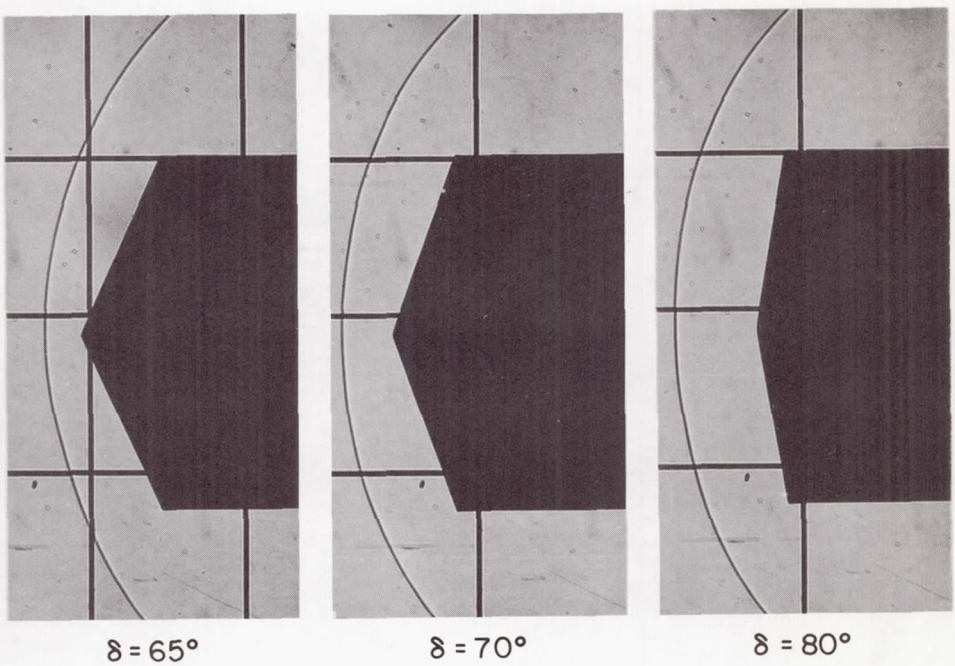

(a) $M_\infty = 8$

Figure 2.- Shadowgraphs of bow wave for conical bodies with semivertex angles from 52° to 90°.

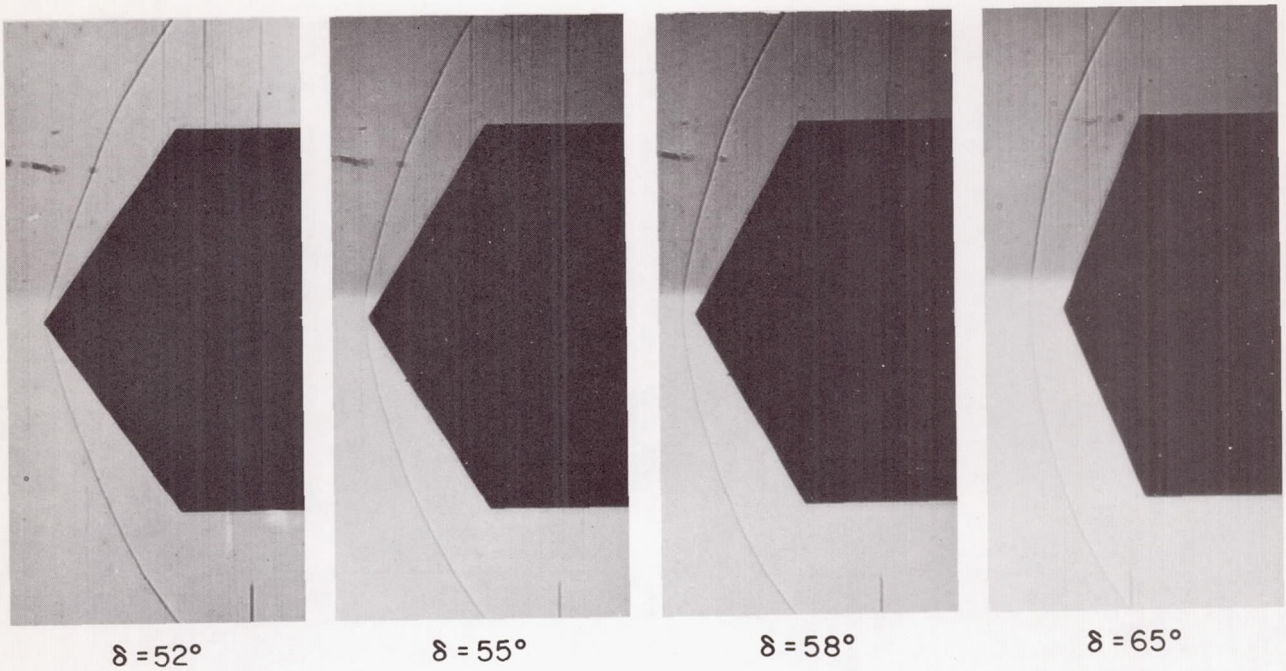

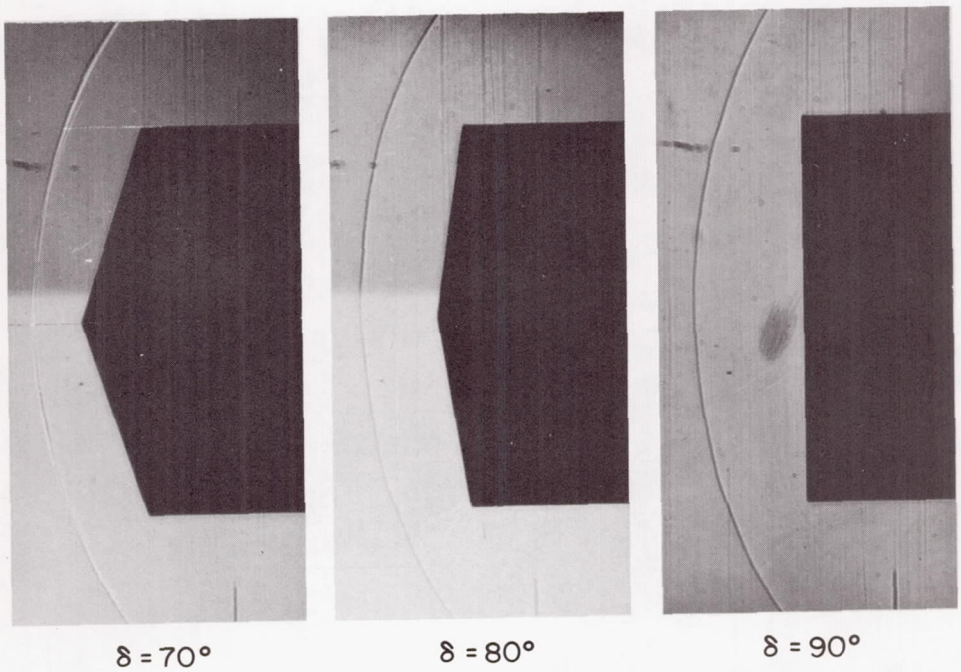

(b) $M_\infty = 20$

Figure 2.- Concluded.

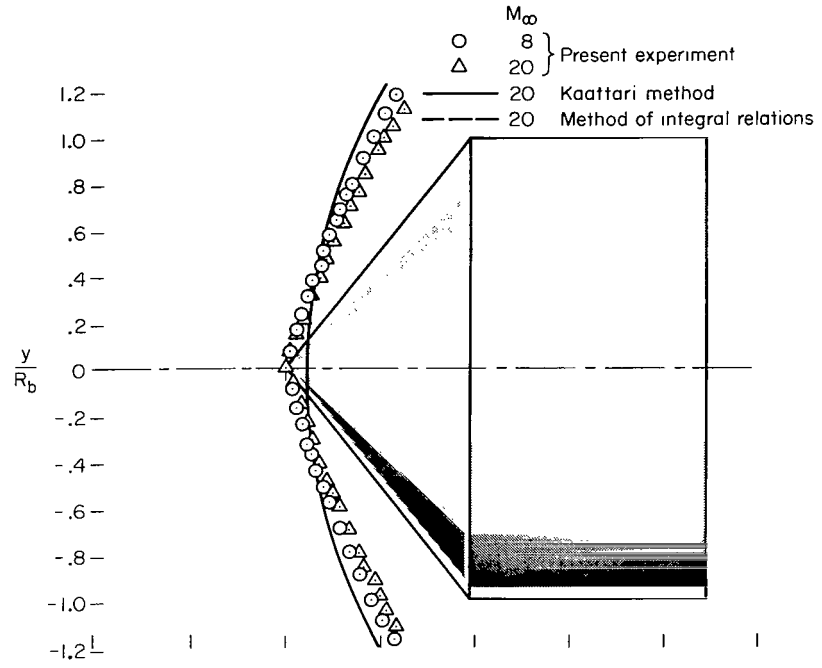

(a) $\delta = 52^\circ$

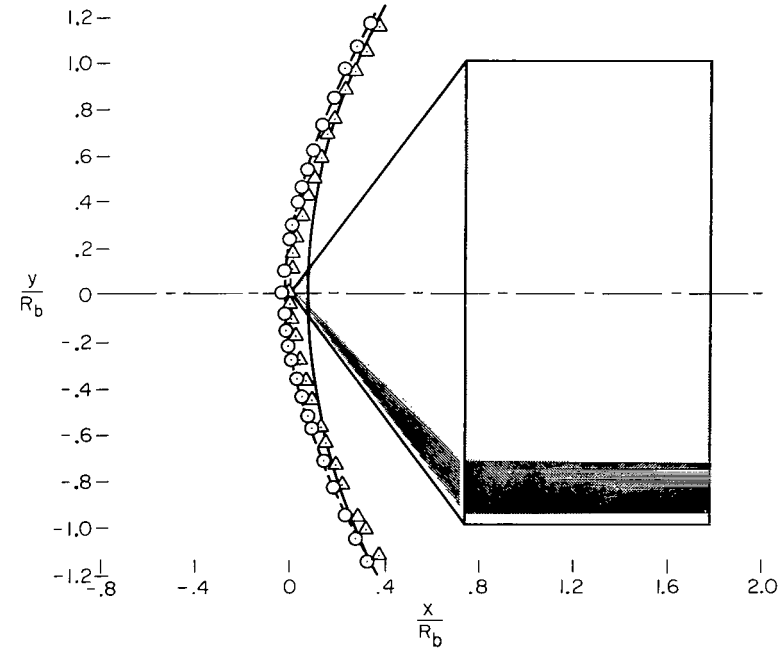

(b) $\delta = 55^\circ$

Figure 3.- Comparison of shock traces from shadowgraphs with approximate prediction methods.

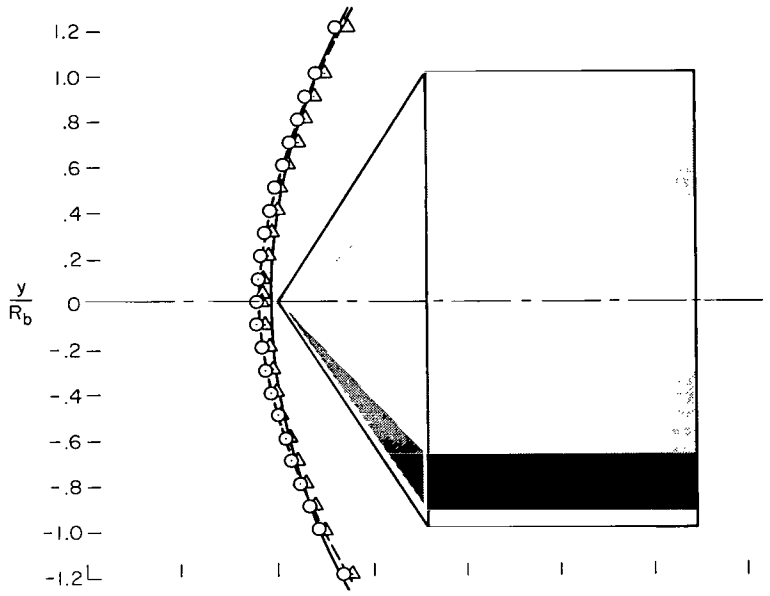

(c) $\delta = 58^{\circ}$

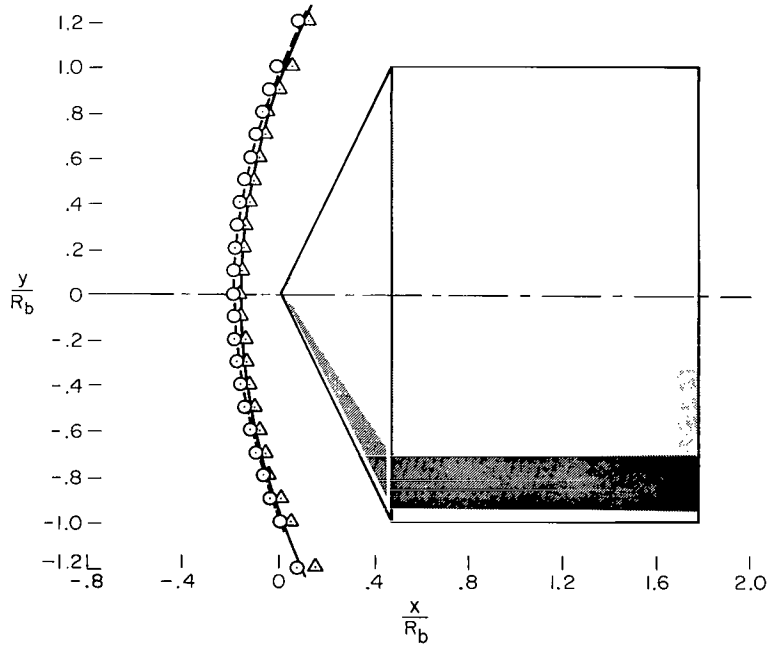

(d) $\delta = 65^{\circ}$

Figure 3.- Continued.

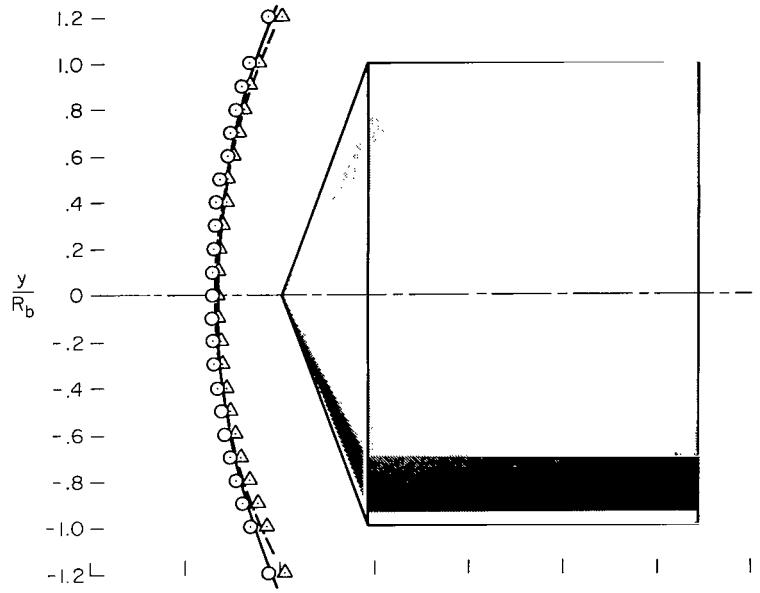

(e) $\delta = 70^{\circ}$

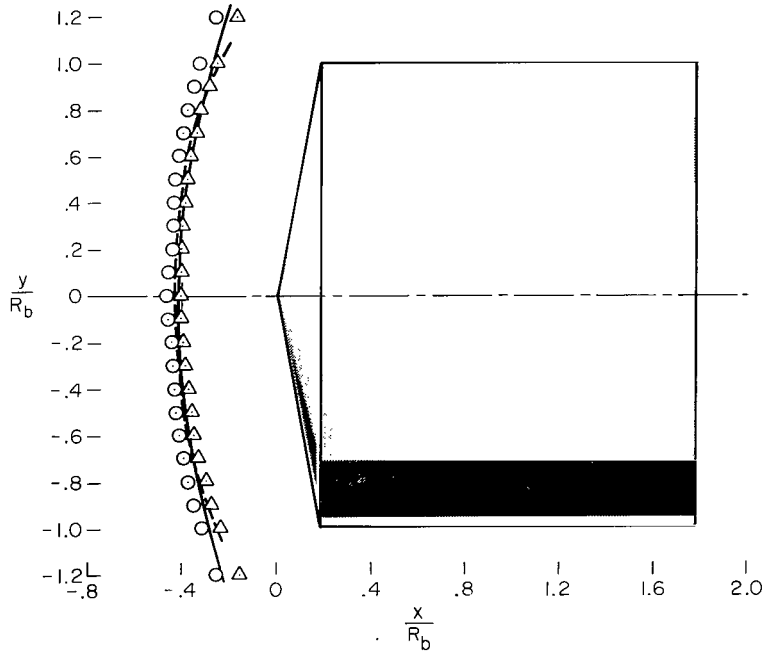

(f) $\delta = 80^{\circ}$

Figure 3.- Continued.

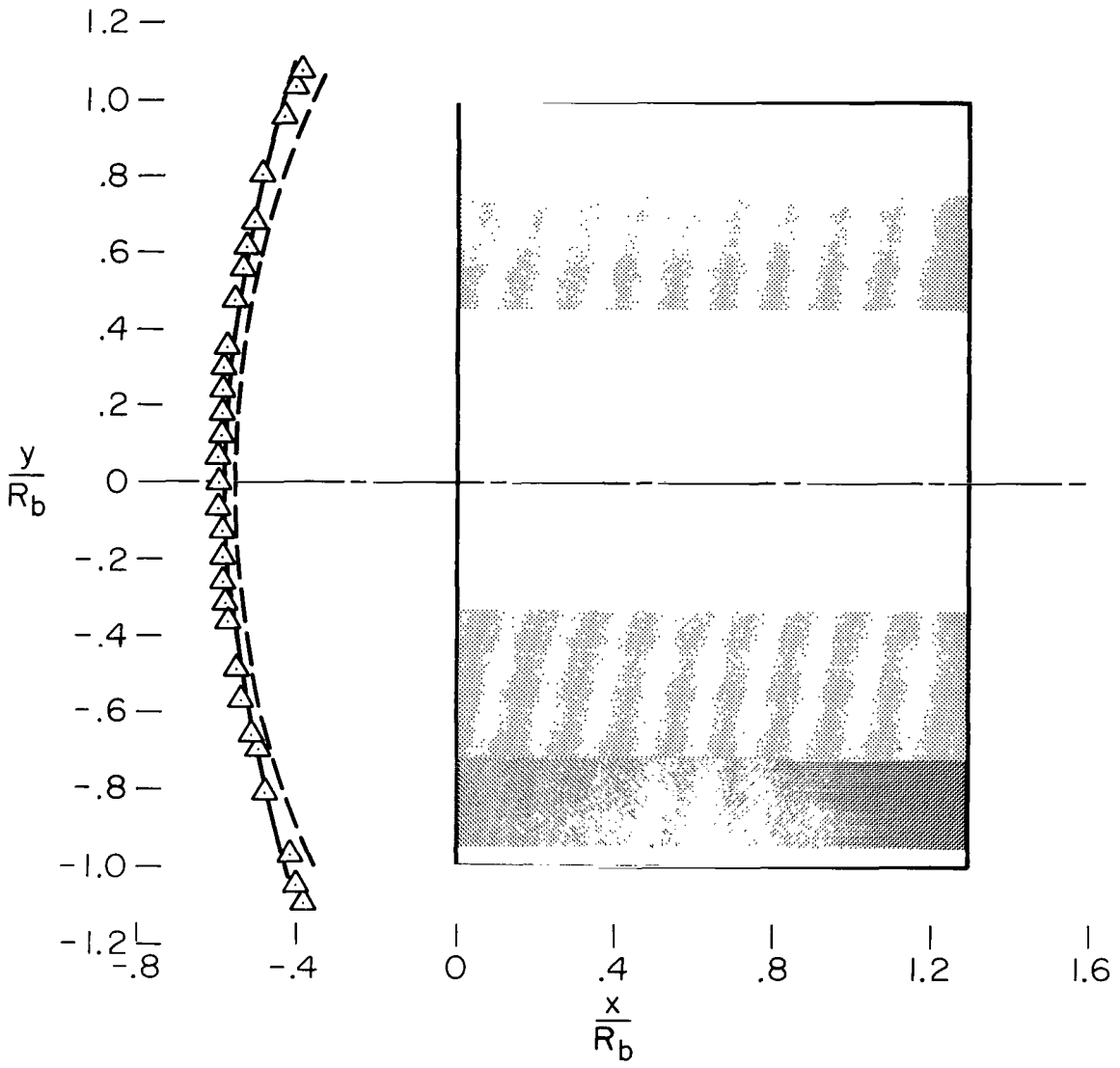

(g) $\delta = 90^{\circ}$

Figure 3.- Concluded.

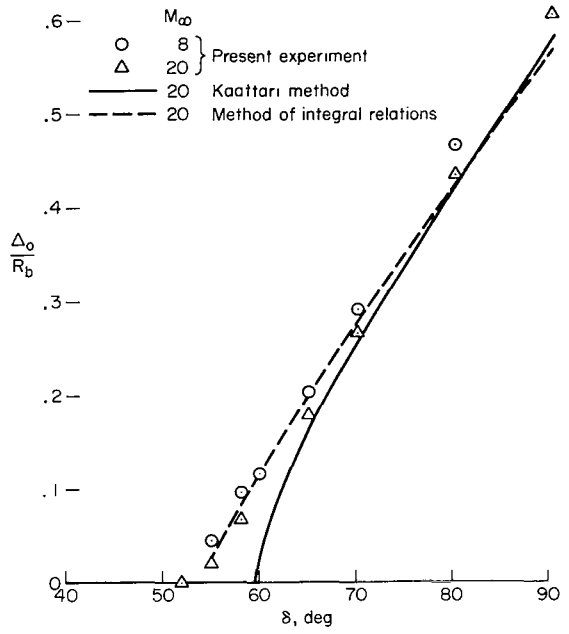

Figure 4.- Variation of centerline shock standoff distance with cone angle.

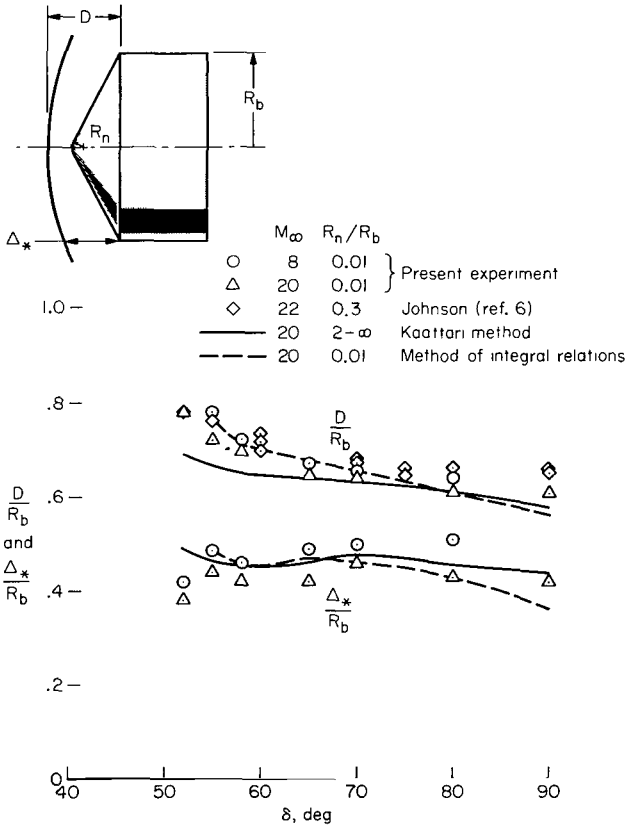

Figure 5.- Variation of shock standoff distance opposite sonic point with cone angle.

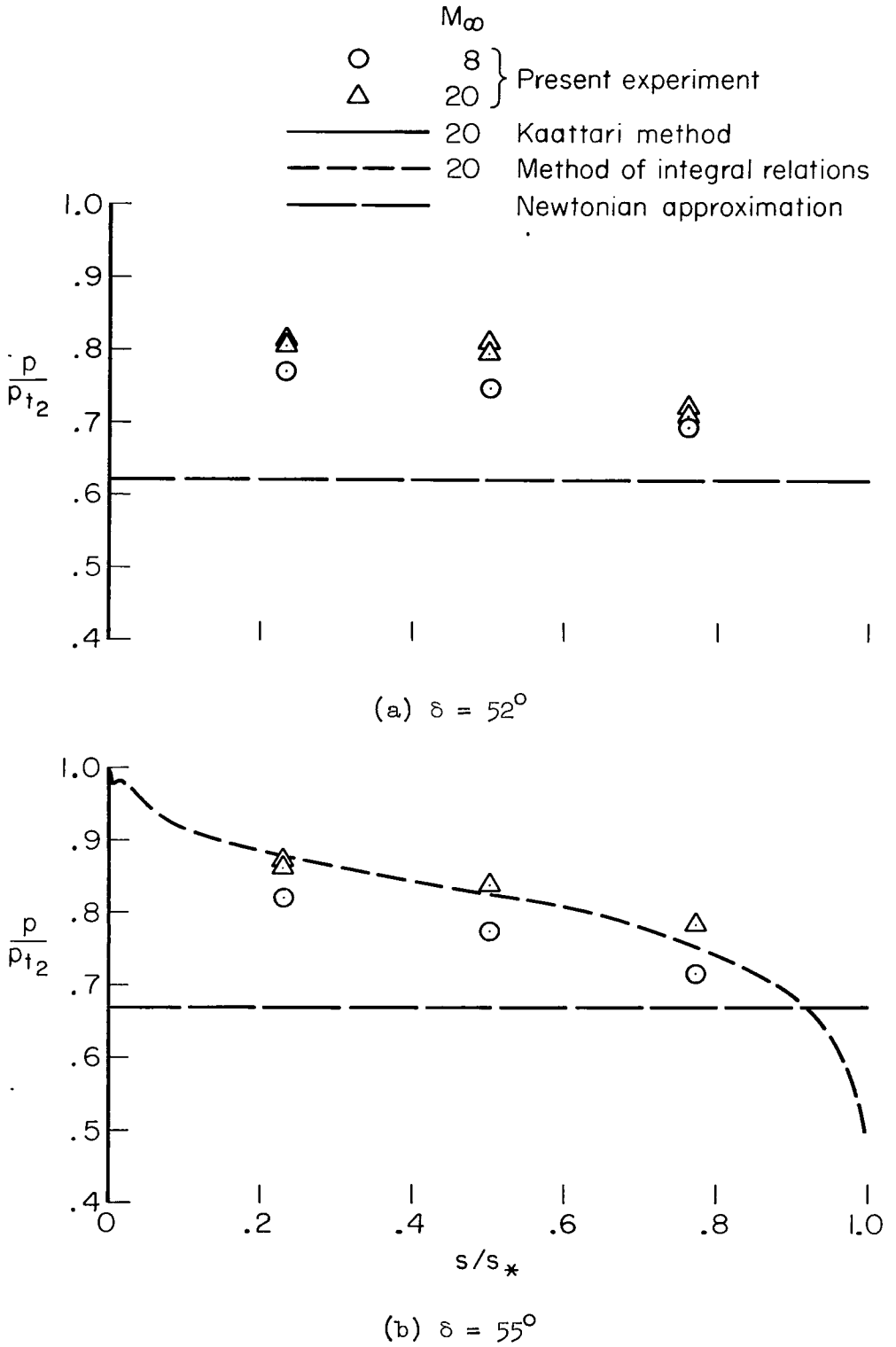

Figure 6.- Pressure distribution on surfaces of large-angle cones in helium.

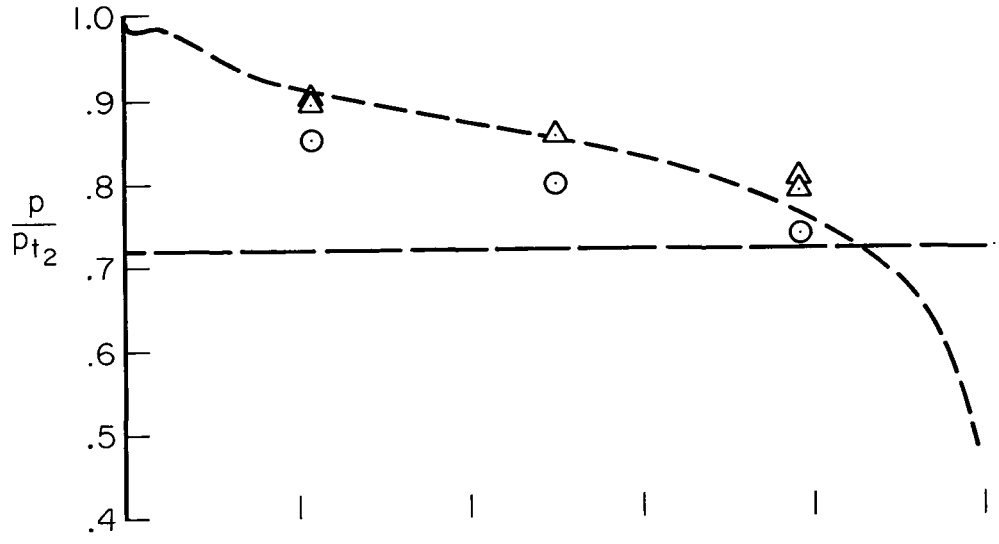

(c) $\delta = 58^{\circ}$

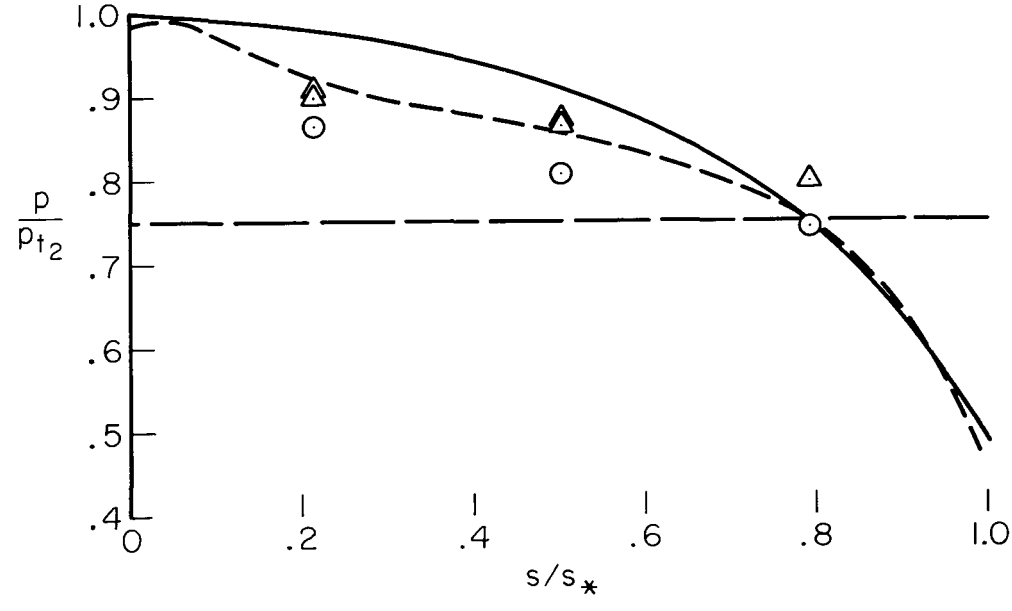

(d) $\delta = 60^{\circ}$

Figure 6.- Continued.

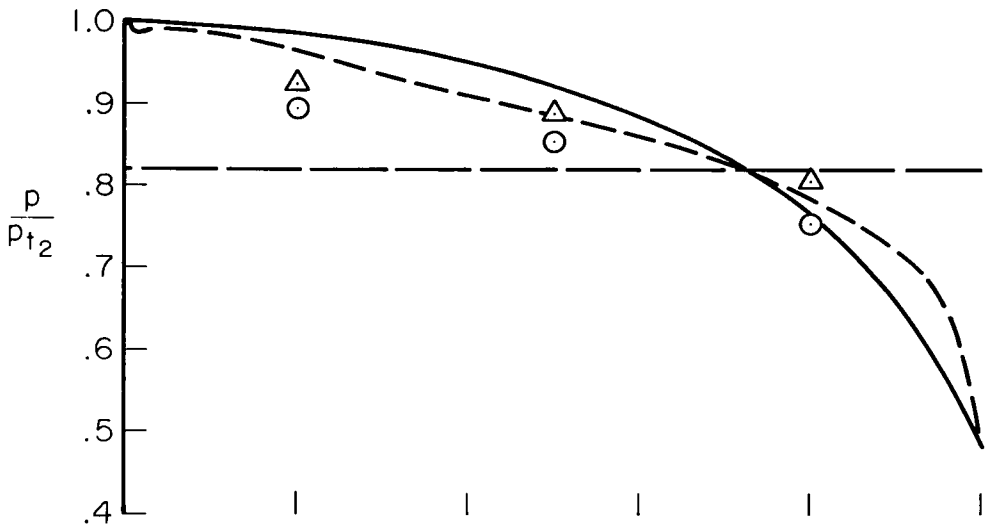

(e) $\delta = 65^{\circ}$

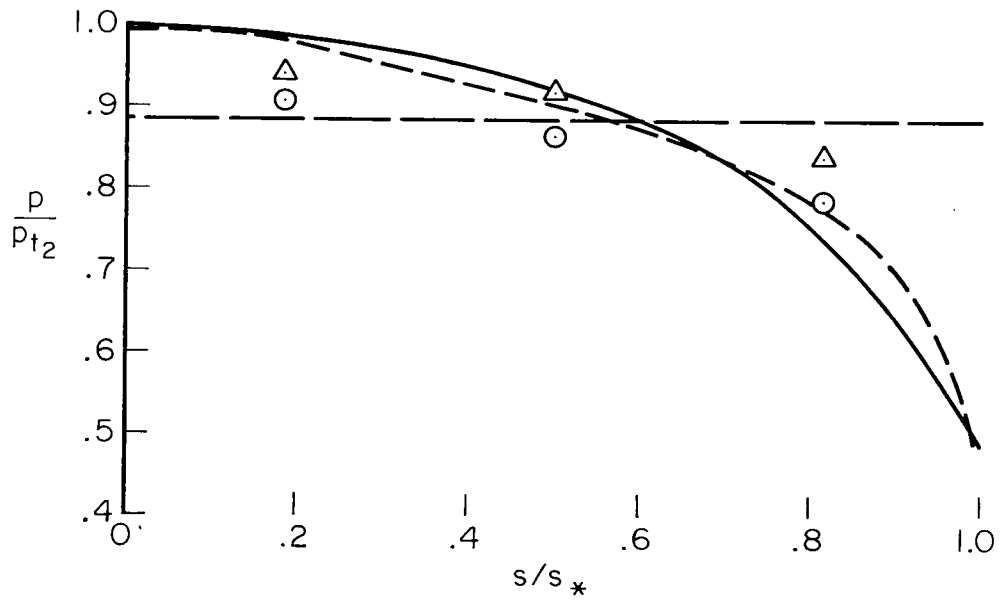

(f) $\delta = 70^{\circ}$

Figure 6.- Continued.

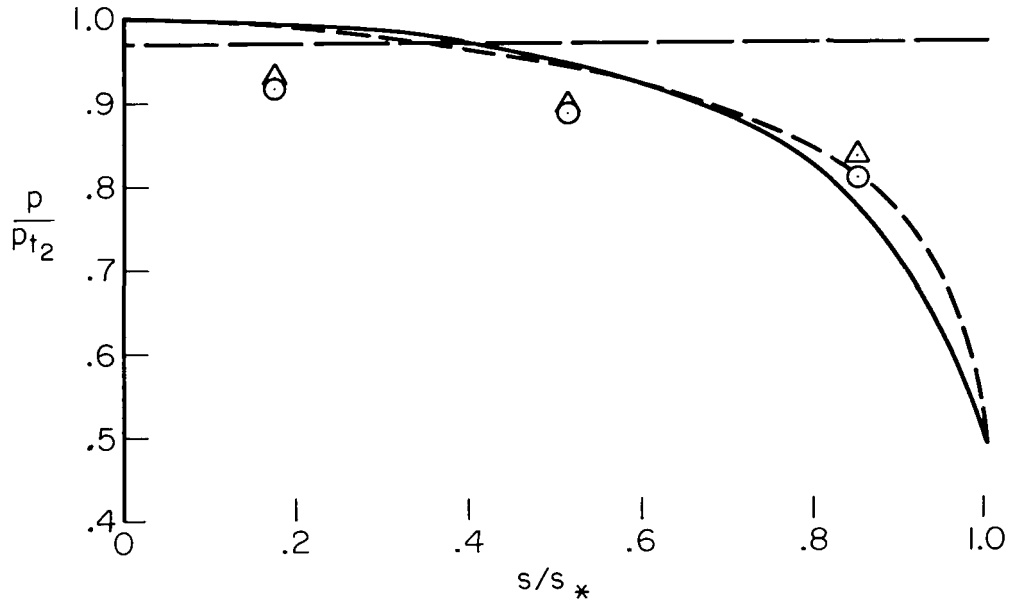

(g) $\delta = 80^{\circ}$

Figure 6.- Concluded.

NASA-Langley, 1969 — 1 A-3278

NATIONAL AERONAUTICS AND SPACE ADMINISTRATION
WASHINGTON, D. C. 20546

OFFICIAL BUSINESS

FIRST CLASS MAIL

POSTAGE AND FEES PAID
NATIONAL AERONAUTICS AND
SPACE ADMINISTRATION

POSTMASTER: If Undeliverable (Section 158 Postal Manual) Do Not Return

"The aeronautical and space activities of the United States shall be conducted so as to contribute . . . to the expansion of human knowledge of phenomena in the atmosphere and space. The Administration shall provide for the widest practicable and appropriate dissemination of information concerning its activities and the results thereof."

—NATIONAL AERONAUTICS AND SPACE ACT OF 1958

NASA SCIENTIFIC AND TECHNICAL PUBLICATIONS

TECHNICAL REPORTS: Scientific and technical information considered important, complete, and a lasting contribution to existing knowledge.

TECHNICAL NOTES: Information less broad in scope but nevertheless of importance as a contribution to existing knowledge.

TECHNICAL MEMORANDUMS: Information receiving limited distribution because of preliminary data, security classification, or other reasons.

CONTRACTOR REPORTS: Scientific and technical information generated under a NASA contract or grant and considered an important contribution to existing knowledge.

TECHNICAL TRANSLATIONS: Information published in a foreign language considered to merit NASA distribution in English.

SPECIAL PUBLICATIONS: Information derived from or of value to NASA activities. Publications include conference proceedings, monographs, data compilations, handbooks, sourcebooks, and special bibliographies.

TECHNOLOGY UTILIZATION PUBLICATIONS: Information on technology used by NASA that may be of particular interest in commercial and other non-aerospace applications. Publications include Tech Briefs, Technology Utilization Reports and Notes, and Technology Surveys.

Details on the availability of these publications may be obtained from:

SCIENTIFIC AND TECHNICAL INFORMATION DIVISION

NATIONAL AERONAUTICS AND SPACE ADMINISTRATION

Washington, D.C. 20546